Original Research Article: full paper

(2022), «EUREKA: Life Sciences»
Number 4

MATHEMATICAL MODELING OF DRINKING WATER AVAILABILITY IN KHARKIV REGION (UKRAINE) AT DIFFERENT DYNAMICS OF GLOBAL CLIMATE WARMING

Nataliy Rychak
Institute of Ecology[1]

Natalya Kizilova✉
Department of Applied Mathematics[1]
n.kizilova@gmail.com

[1]*V. N. Karazin Kharkiv National University*
4 Svobody sq., Kharkiv, Ukraine, 61022

✉**Corresponding author**

Abstract

Water purity and availability determines health and life quality of humans, biodiversity and existence of plants and animals. The results of global climate change have been registered all over the world as progressive warming with fast heat waves, accelerated glacier ice melting, variations in the global ocean streams and heat balance, droughts and lack of drinking water, damage to plants and animals. Mathematical modeling of the water exchange in local ecosystems is a very important constituent of detailed analysis of different scenarios of water availability at various trends in the weather change.

The work is aimed at mathematical modelling of water balance in an urban ecosystem accounting for global climate changes. A brief review of the models is presented, and a synthetic model for the water balance on the urban territory of Kharkiv city (Ukraine) based on the statistical dependencies, compartmental system dynamics approach and hydrological equation with probabilistic description of the input parameters is developed. The monthly and year averaged temperature and precipitation curves, time series on downpours, droughts and storms over the Kharkiv region and Kharkiv city during 1908−2012 years were collected from the open databases and analyzed. Gradual increase in the annual temperature was confirmed.

Different scenarios of the regional development (population growth and industry development with increased water demands) and weather changes were tested, and availability of water has been estimated. It was established by numerical simulations, the water insufficiency in the region in 2040 could reach 10−17 % if the mean annual air temperature increases in 0.5−2.5 °T. This will cause damage for plants, animals, and human health. The obtained results are important for decision making by official planning authorities and regional administration.

Keywords: climate warming, drinking water availability, river system, hydrology, mathematical modeling.

DOI: 10.21303/2504-5695.2022.002610

1. Introduction

Global climate changes, which are associated with progressive warming and decreasing air humidity, ice melting in Antarctica and Greenland, atypical southern oscillations El Niño, elevation of methane release into the atmosphere, and many other hazards have lead to irreversible changes in nature: biodiversity loss in ecosystems, sudden downpours and floods, forest fires and droughts, lack of food and drinking water in the developing countries [1–3]. Recently, a disastrous melt rate of glaciers has been recorded in Switzerland [4]. This year, low snowfall and persistent heat waves caused a 6 % loss of glaciers in the Alps. Regular reports on the outcomes of global climate change appear in mass media of all the developed countries, and significant efforts are made in understanding the physical phenomena and quantitative predictions based on mathematical models [1]. It was shown, the glacier melt, heavy rains and other disasters can be explained with hydrological models [5] and general energy balance algorithms [6] because the surface water reservoirs, surface runoff, snow and ice deposits are interconnected with groundwater via the porous soils (**Fig. 1**). The hydrological models are based on the systems of ordinary differential equations (ODE) for time dependencies of the water mass in each compartment of the model (Precipitation→Surface

runoff→Intermediate runoff→Subbase runoff→Base flow) or on the systems of partial differential equations (PDE) for the pressure, flow, stress, concentrations, temperature distributions in different layers (atmosphere, vegetation cover, surface, soil, waterproof rock). Since each component in (**Fig. 1**) is considered as a single compartment, the mathematical equations described the water balance between them compose a compartmental model.

Different discrete, continual and synthetic models of river beds in connection with precipitation, percolation in soils and groundwater flows have been proposed taking into account geometry of the riverbed, composition of bottom sediments, water flow velocity, surface runoff, and other parameters. These models are widely used to calculate the removal of bottom sediments and channel migration, water quality and pollution transfer, ecological expertise of the ecosystem, and other practical problems [7–9]. Mathematical modeling and numerical calculations of the velocity field, vorticity, friction stresses and other hydrodynamic parameters make it possible to assess the risks of coastline erosion, bottom erosion, to identify areas with slow currents, in which, due to insufficient water circulation, the bottom will become overgrown and the water quality will deteriorate.

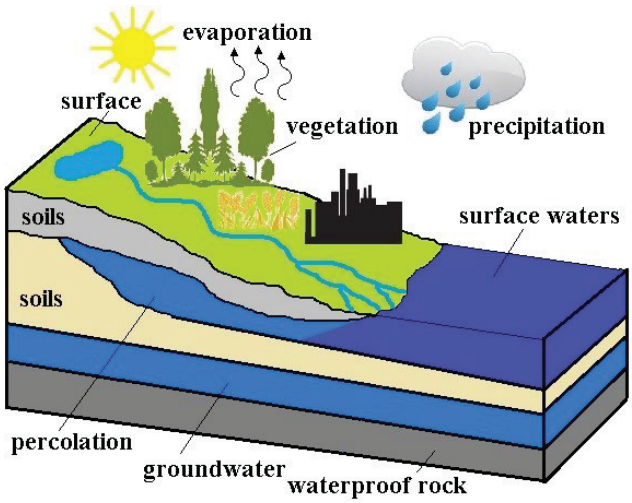

Fig. 1. Water exchange system between the atmosphere and surface

In this paper the results of mathematical modeling and calculations of water velocity, pressure distributions, friction and other hydrodynamic parameters in the system of rivers on the territory of city Kharkiv that contribute to the riverbed migration, its overgrowth, deterioration of water quality and problems in drinking water availability are presented. The results are used for mathematical modeling of water availability in the city at different scenarios of the city development, demography and climate changes.

2. Materials and methods

Mathematical modeling of water dynamics in an urban area (**Fig. 1**) aimed at prognosis of the drinking water availability is used as a powerful method for complex long-range prognoses. A synthetic model based on several types of the developed models has been elaborated in the work.

The most common mathematical models use regression dependencies in the form of statistically reliable trend curves $X(t)$, where X is a quantitative indicator of precipitation (rain, snowfall, hail, ice, etc.), t is time (in months, years). There are statistical approximations for various countries (regions, lands, cities), including Ukraine [10]. Based on the observation data on the territory of Ukraine, during the period 1986–2010, there were 1,335 downpours, 237 snowfalls, 131 hailstorms, 398 cases of strong wind, 164 squalls, 249 blizzards, 3 sandstorms, 70 complex ice deposits; a total of 3031 adverse events the majority of which were showers (52.9 %). Corresponding regression dependences for each of the areas are given in [11] for heavy and dangerous downpours and rains,

taking into account recurrence, intensity and season. Recently, similar statistical data for 2010–2020 have appeared, which have other regressive dependencies due to climate warming [12]. These data are very important for use in mathematical models, but the stochastic nature of bad weather conditions is more accurately described using probabilistic models.

The concept of probability of maximum amount of precipitation (V_{max}) for a certain time that is physically possible for a given size of the storm area in a certain geographical location at a certain time of the year has been introduced [13]. The simplest mathematical model introduces the dependence of the average volume of surface water V_S (m^3) on the mean precipitation volume V_V (m^3) in the form

$$V_S = k_{VS} V_V + \varepsilon_S, \tag{1}$$

where k_{VS} is a dimensionless coefficient, ε_S is probable deviation from the average values, which are calculated based on $V_{\max}$.

Similar dependence for the volumetric rate of the surface flow Q_S (m^3/s) can be written as [13]:

$$Q_S = \kappa_{VS} Q_V \frac{T_V}{T_S} + \varepsilon_Q, \tag{2}$$

where T_V, T_S are time durations of the precipitation and surface runoff, κ_{VS} and ε_Q are similar to the coefficients in (1).

The total mass of pollutants M_S (kg) in surface waters after precipitation is calculated as

$$M_S = C_V V_V + \varepsilon_M, \tag{3}$$

where C_M (kg/m^3) is the concentration of the pollutants in surface waters, ε_M is similar to the corresponding coefficients in (1), (2).

In urban areas, precipitation washes away both transport pollution (fuel, oils, heavy metals, etc.) and agricultural pollution (fertilizers, nitrates, nitrites, etc.), and can also cause overflow of drains and ingress of wastewaters into the surface waters, which is dangerous for the quality of both drinking and technical water [2, 3, 9]. Decision-making on water management is usually carried out after evaluating the values of V_S, Q_S, M_S in comparison with the volumes of reserve possibilities of local flows. The value k_{VS} is obtained from regression dependences for this area; the values V_V, T_V, T_S and ε_S, ε_Q, ε_M are usually computed from the measurement data and probabilistic models, accordingly [13].

The probabilistic models are based on determination of probability of the distribution of surface runoff $\{V_S, Q_S\}(t,x,y,z)$ from a given "point" source $\left\{V_V, Q_V\right\}\left(t, x_j, y_j, z_j\right)_{j=1}^{n}$ of precipitation in a defined area $\{S: x\in[x_1,x_2]; y\in[y_1,y_2]; z\in[z_1,z_2]\}$. Ordinary rains, showers, snowfalls, etc. are distributed sources, which requires the determination of spatio-temporal functions $\{V_V, Q_V\}\{t,x,y,z)$ from all distributed sources j=1,…,n.

One of the methods is based on stochastic storm transposition (SST), which combines the probabilities of "arrival", "accumulation" and "transfer" of precipitation even in an area that lies outside the precipitation zone, but has surface runoff from it based on the probability theory. The SST method assumes that storms occur with equal probability at any point in the transposition domain. The probability of the event that a given precipitation area (S) with a certain catchment will be overloaded with precipitation takes into account the localization of storm centres that led to an excess of precipitation in the vicinity of S. The probability of this event is calculated as the ratio of the incidence plane to the plane of the transposition region, which is estimated by normal distribution of the transposition over a large number of grid cells on and near the plane [14]. The second method, which is based on "stochastic storm regression" (SSR), combines point precipitation frequency curves with regression estimates of local and accumulated precipitation on the area. Precipitation maxima are generated by stochastic sampling of independent variables, where the necessary probabilities of exceeding the precipitation level are obtained using the general probability theorem [15].

Many mathematical models combined SST and SSR have been developed [13]. According to the probabilistic models, instead of (1) one has

$$V_S = \sum_{j=1}^{k} k_j V_{Vj} + \varepsilon_S, \tag{4}$$

where k_j are regression coefficients for the most probable and influential precipitations j=1,…,n (prime key sites, PKSs); similar generalizations can also be written instead of (2), (3).

The curve of the precipitation frequency over a natural habitat territory is derived using the general theorem of probability theory, in which the probability that a certain amount of precipitation V_S over the territory S is equal to or exceeds V* is determined by the probability of a point amount of precipitation in a key area [13]

$$P\left(V_S \geq V^*\right) = \sum_{j=1}^{k} P\left(V_S \geq V^* \mid V_{Sj}\right) \cdot P\left(V_{Sj}\right). \tag{5}$$

The parameters in (5) are subject to epistemic uncertainty arising from the finite nature of the available data. This uncertainty can be characterized using the parametric bootstrap method, and the uncertainty in the correlation between precipitation maxima at PKSs is based on the assumption that the transformation of the sample correlation coefficient is distributed with a standard error [16]. For the purpose, the relations used to represent hydrological variability are randomly selected to reflect the uncertainty associated with their parameterization.

The probability that the average amount of precipitation V_S exceeds the predicted amount V^* can be estimated using the general integral [14, 16]

$$P\left(V_S \geq V^*\right) = \int_f P\left(V_S \geq V^* \mid f\right) \int_{As} p\left(f \mid A_s\right) p\left(A_s\right) \mathrm{d}A_s \mathrm{d}f, \tag{6}$$

where f – storm precipitation depth of the area A_s; $P(V_S \geq V^* \mid f)$ is the conditional probability that the average catchment has the area $V_S \geq V^*$ when the precipitation depth is f; $P(f \mid A_S)$ is the storm probability density over the area A_s in the transfer area with the precipitation depth f; $p(As)$ is the probability density function of the samples of storm zones (assumed to be uniform).

Therefore, statistical data on the distribution of rainfall in terms of their intensity and duration along a grid generated over the area of interest, are the main inputs for both SST and SSR methods. Standardization and bias-correction of the precipitation grids is carried out by regression and probability methods [16].

Fluid dynamics equations based on the laminar (slow flows) or turbulent (fast flows) models for water movement in the riverbeds with surface runoff, Darcy's law for the water percolation in the porous soils are used for computations of the hydrostatic pressure and flow velocity. The advection-diffusion equations for concentrations of different pollutants are used for computations of the concentrations when the flow velocities are computed and the sources of the pollutants are known. A detailed review of the equations and examples of their solving are thoroughly discussed in [9, 17].

The simplest 2D hydrological model of river flows is based on the equation

$$\frac{\partial h}{\partial t} + div\left(\vec{q}\right) = q_c, \tag{7}$$

where $h = z + H + \dfrac{v^2}{2g}$ is the dynamic head, v is the flow velocity, g is the gravitational acceleration, $H(x)$ is the river depth profile, z and x are vertical and longitudinal coordinates, q_c are mass sources distributed along the riverbed (tributaries, rainfalls, snow melting, outlets), $\vec{q} = -kK\nabla h$ is the mass

flux, $k=H^{5/3}$ is the hydraulic conductivity of the channel profile, $K=\sqrt{S}/m$ is friction over the wetted surface, $S=(\partial h/\partial x)^2+(\partial h/\partial z)^2$ is the slope, m is the Gauckler-Manning roughness coefficient.

More detailed 3D computations can be carried out on the incompressible Navier-Stokes equations

$$div(\vec{v})=q,\ \ \rho\frac{d\vec{v}}{dt}=-\nabla p+\mu\Delta\vec{v}+\rho\vec{g}, \tag{8}$$

where ρ and μ are density and viscosity of the fluid, p is the hydrostatic pressure, q are the water sources along the riverbed.

The boundary conditions for (8) are

$$\vec{v}\big|_{\Gamma 1}=0,\ \ p\big|_{\Gamma 2}=p_{atm}, \tag{9}$$

where p_{atm} is the atmospheric pressure, Γ_1 and Γ_2 are wetted and free surfaces of the riverbed, respectively.

When both positive (bottom springs, tributaries, rainfalls, outlets) and negative (channels, percolation sites, water intake) are presented, their distributions must be taken from the measurement data and approximations as a function $q=q(x,y,z)$. Transfer of the pollutants can be modeled by convection-diffusion equations for their concentrations. The temperature balance in the system can be modeled based on the heat equation. Then the temperature dependent evaporation rate from the free surface Γ_2 must be added.

For the riverbeds with arbitrary geometry the problem (8), (9) can be solved numerically by the finite element or finite volume methods. A reasonable simplification can be introduced by averaging of (8) over the cross-section of the riverbed. The resulting 1D equations have exact solutions as a piecewise continuous function that is useful for preliminary estimations of the problem solution and for reliable validation of more detailed 3D models.

3. Results and discussion

According to data available from the World Resources Institute, a large part of the territory of Ukraine has a high (3–4) or medium (2–3) stress index for water supply, the highest level of drought (0.8–1) and quite high (3–5) index of coastal floods [12]. Values of average, minimum and maximum monthly temperatures in the Kharkiv region during the year are shown in **Fig. 2**. The lowest and highest temperatures for the entire observation period were recorded in 1893–1964 and 1931–2015, respectively, which indicates a noticeable climate warming in the region. Similar conclusions can be drawn for other regions of Ukraine.

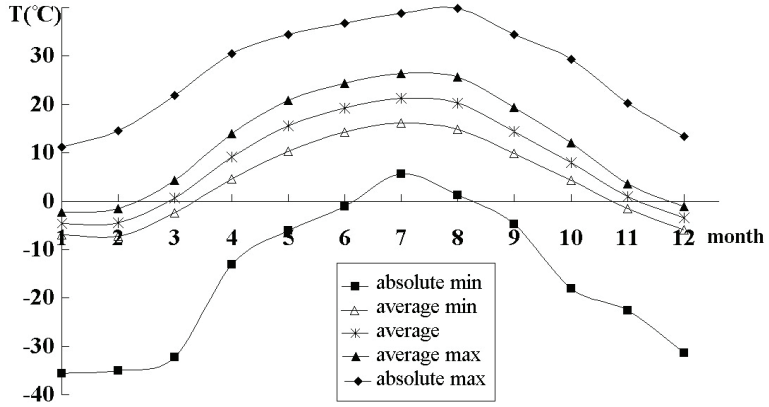

Fig. 2. Values of average and absolute minimum and maximum air temperatures in different months in Kharkiv region

Therefore, development and analysis of mathematical models of water resources management accounting for peculiarities (urbanized, agricultural, tourist, etc.) of the cities and regions of Ukraine is very important. This type of modeling has been done for many cities and regions USA, Europe and Africa [11, 18, 19], while there is a lack of the models developed for the Ukrainian water resources.

City Kharkiv is located around the junction of the rivers Kharkiv, Lopan and Udy (**Fig. 3, *a***). The top view geometry of the riverbeds has been taken from satellite images (surface geometry, temperature, soil use, etc.) collected in the open access online resource Google Earth Engine. The 3D surface geometry has been determined using online Shuttle Radar Topography Mission (SRTM) data. The locations, depths and compositions of the soils and groundwater layer have been taken from hydrogeological maps. The river bottom profiles have been computed by averaging data during field measurements across the stream (**Fig. 3, *b***). The measurements were carried out in the first decade of June, 2016–2019. A measuring tape with marks located at h=10 cm intervals was stretched between the left and right banks of the river perpendicular to its flow direction. The boat with a depth measuring system moved gradually along the rope, and the depth of the river was determined near each mark. The collected data were smoothed and the evolution of bottom profiles has been analyzed based on the data on the snow melt and rainfall dynamics during the spring time. The measurement results for four sections marked in **Fig. 3, *b*** are presented in **Fig. 4.** The slope along the channel and the velocity of the river flow along the middle line, near the left and right banks, were also measured. The dynamics of changes in the depth and width of the river, associated with low or high snow level in winter, and dry or rainy spring, as well as changes in bottom profiles associated with the transfer of sediments and channel overgrowth has been studied.

As it was recorded in all the profiles, the right bank is steeper than the left, in accordance with the Coriolis force in the Northern hemisphere (**Fig. 4**). However, the degree of steepness of the right and left banks varies due to erosion and transfer of bottom sediments. The river bed in the studied area is twisting; the river turns twice to the left and once to the right at the angles 124.8°, 116.7°, 144.3°, respectively. Due to the flow inertia, the water mass will be swept towards the right, right and left bank at three corresponding turns, causing additional erosion of the appropriate banks and transfer of bottom sediments. A detailed answer to the question of the further evolution of the channel and the dependence of this process on the level of precipitation and air temperature changed by the global climate warming can be given based on mathematical modeling of the water circulation in the whole system (**Fig. 1**).

Equation (7) describes quite well the change in the flow velocity for slightly meandering rivers, however, in the case under consideration, the presence of several successive multidirectional turns leads to the fact that the inertia of the flow and its drift in the direction transverse to the flow significantly affect the hydrodynamic parameters. Therefore, more accurate calculations on a 3D model accounting the real river bottom profiles are required.

Based on the results of digitizing the boundaries of three riverbeds inside the administrative boarders of the city Kharkiv, a 3D geometric model and a homogeneous grid were built. Due to big difference in scales in the longitudinal (0x, 0y ~10 km) dimensions and the depth (0z, ~100 m), a small part of the river system is presented in **Fig. 5, *a*.** The uniform mesh in one of the cross-sections and the mesh of the surface are presented in **Fig. 5, *b*, c**, accordingly.

The total number of nodes and finite elements was 12643170 and 6713218, respectively. The chosen values were determined by obtaining a mesh-independent numerical solution. Computational fluid dynamics (CFD) simulations have been carried out in AnSys Fluent 2021 academic version. The distributed sources $q(x,y,z)$ have been determined as user-defined functions (UDF). The gravity vector was determined according the slope of the landscape. The flow inlet boundary conditions (9) have been assigned in the locations of the inlets of three rivers at the boarders of the city Kharkiv. Convergence of the computations has been monitored by both residuals and total mass flow rate in the river system.

The characteristic values of the Reynolds number for the case under consideration were Re=103–104; therefore, models of both laminar and turbulent flows (Spalart-Allmaras model) with a second-order numerical scheme and calculation accuracy of 10^{-5} were used.

a

b

Fig. 3. Geometry of the water system: *a* – rivers Kharkiv (1), Lopan (2) and Udy (3) on the territory of the Kharkiv city; *b* – a river segment with locations 1–4 for the bottom profile measurement sites

The results of calculations of the velocity field are presented in **Fig. 6, *a*** as the streamlines on the free surface coloured in accordance with the magnitude of the velocity for the piece of total geometry shown as example in **Fig. 3, *b***. The areas of accelerated flow in the narrowest cross sections of the channel are clearly visible, as well as areas of separation of streamlines and areas with stagnant eddy circulation near the widened zones of the channel. Due to low flow rates, these areas are the most likely to be overgrown with various aquatic vegetation and poor water quality. In accordance with geophysical data, in the areas with accelerated flow the bottom sediments are transferred to the areas with lower flow by the shear forces, which further worsen the circulation and contributes to the overgrowth of the entire bottom. At the channel turns, the central core of the flow drifts to one of the banks, which leads to the erosion of the coastline, which is noticeable on the top view images of the streamlines (**Fig. 6, *b*)** and shear stress over the bottom (**Fig. 6, *c***). In areas with sharp differences in the channel width, as well as after the turns, there are increased friction values up to σ=2.73 kPa, which can cause both erosion of the coastline and movement of bottom sediments. The obtained numerical results are of the same order of magnitude for the laminar flow and the Spalart-Allmaras turbulent models.

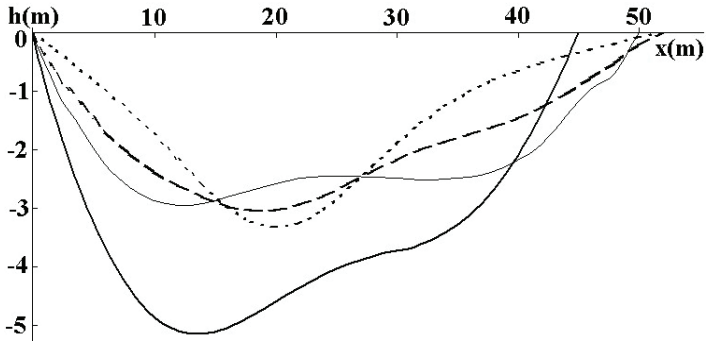

a

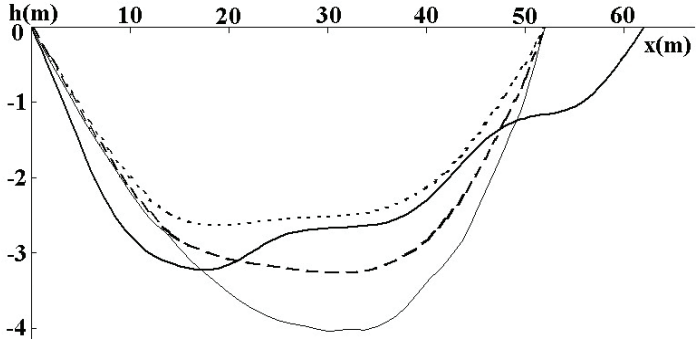

b

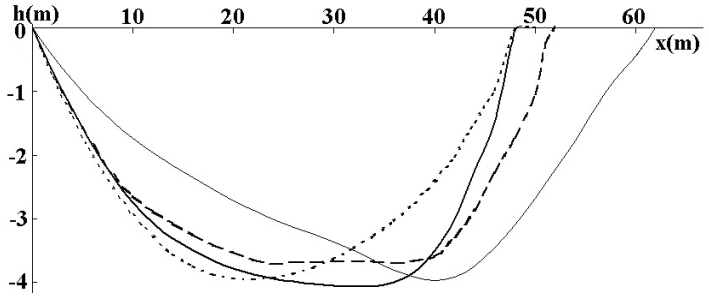

c

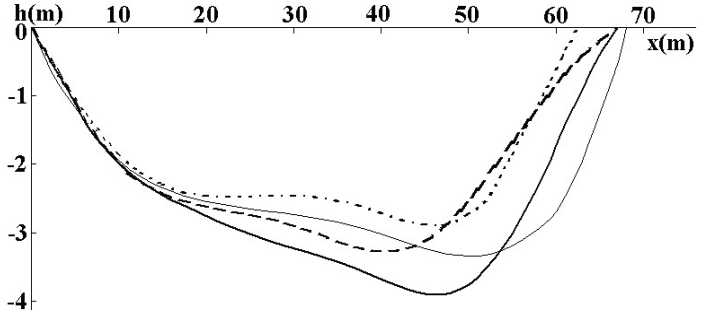

d

Fig. 4. River bottom profiles along 4 cross sections (**Fig. 3, *b***) measured in 2016 (solid line), 2017 (thin line), 2018 (dotted line), 2019 (dashed line): *a* – section 1; *b* – section 2; *c* – section 3; *d* – section 4

Comparative analysis of the computed and calculated flow velocity values revealed a good correspondence between the calculated and measured values (**Table 1**) that confirms accuracy and reliability of the developed model, and its ability to quantify the results of various engineering hydrophysical structures for the coastline protection measures and control over erosion and gradual evolution of the river basins.

The results of CFD computations for the weather conditions (functions $q(t)$ in (8)) detected in 2016–2019 over the territory of Kharkiv city has been averaged of each cross-section along the river systems, and the resulting volumetric flow rates $Q(t)$m/s have been used as the surface water component in the general model (4)–(6). This model has been validated by the 2016–2019 meteorological and hydrological data available [20–22]. The data of meteorological prognoses (ThData) for total month-averaged precipitation (in mm) have been smoothed by Bayesian filters and compared to the valued measured by local meteorological stations over territory of Kharkiv region (ExpData). The distributions of ThData versus ExpData before and after the smoothing are presented in **Fig. 7, *a, b*** accordingly. Bayesian filtering produces a much better correspondence between the global predicted and local measured precipitations with lower dispersion. The dispersion in **Fig. 7, *b*** depends on the precipitation area; the prognosis is more accurate for smaller areas (point sources of water).

The measured and smoothed curves for the mean air temperature, humidity, wind direction and intensity, precipitation amount have been approximated by different probability distribution functions (PDF), namely, Gamma (I), Lognormal (II), Normal (III), Weibull (IV), Gumbel (V), Gumbel^{+} (VI) in the form [7, 8, 12, 18]

$$F(V,\alpha,\beta,\zeta)=\begin{cases}\text{I.}\,|\beta|\left(\beta(V-\zeta)\right)^{\alpha-1}e^{-\beta(V-\zeta)},\\ \text{II.}-\left|\log(V-\zeta)-\beta\right|^{2}/2\zeta^{2}\sqrt{2\pi\zeta(V-\zeta)},\\ \text{III.}\,e^{(V-\beta)^{2}/2\alpha^{2}}/\alpha\sqrt{2\pi},\\ \text{IV.}\,(\zeta-1)e^{(V-\alpha)/\beta}/\alpha,\\ \text{V.}\left(e^{-(V-\zeta)/\alpha}/\exp\left(e^{-(V-\zeta)/\alpha}\right)\right)/\alpha,\\ \text{VI.}\,e^{-((1-\beta(V-\zeta)/\alpha)/\beta)},\end{cases}\tag{10}$$

where V is the parameters under consideration, Γ is the gamma-function, α, β, ς are model parameters.

Table 1

The values of the flow velocity v(m/s) near the free surface in the sections 1–4 (**Fig. 3, *b***); the upper and lower values correspond to the CFD and measured values< accordingly

Cross-section	Location	2016	2017	2018	2019
1	Left bank	0.084/0.08	0.096/0.11	0.096/0.12	0.090/0.09
1	Midline	0.380/0.39	0.454/0.42	0.334/0.35	0.431/0.38
1	Right bank	0.125/0.17	0.141/0.13	0.138/0.14	0.133/0.12
2	Left bank	0.278/0.25	0.322/0.35	0.397/0.40	0.303/0.35
2	Midline	0.551/0.48	0.584/0.55	0.612/0.55	0.488/0.45
2	Right bank	0.332/0.35	0.478/0.45	0.528/0.50	0.384/0.40
3	Left bank	0.078/0.10	0.088/0.12	0.092/0.12	0.075/0.08
3	Midline	0.354/0.30	0.403/0.45	0.385/0.41	0.498/0.45
3	Right bank	0.142/0.15	0.128/0.14	0.155/0.14	0.125/0.13
4	Left bank	0.075/0.08	0.082/0.10	0.089/0.11	0.084/0.09
4	Midline	0.332/0.35	0.396/0.40	0.427/0.45	0.406/0.45
4	Right bank	0.136/0.12	0.139/0.15	0.122/0.14	0.120/0.13

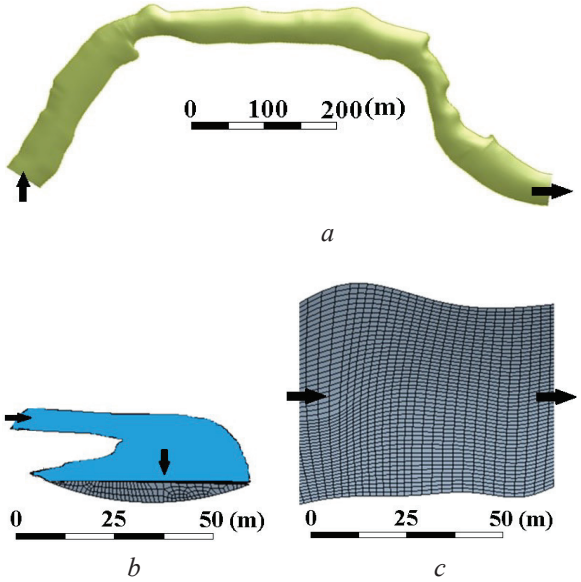

Fig. 5. An example of the 3D model of the river basin: *a* – bottom view of the segment; *b* – mesh a cross section (side view); *c* – mesh on the free surface (top view)

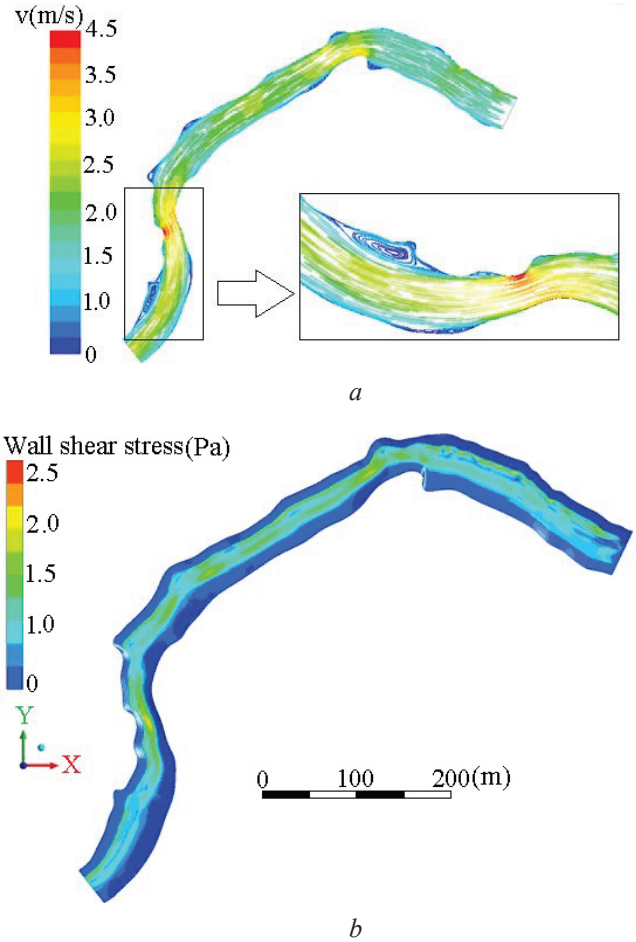

Fig. 6. Computational fluid dynamics results: *a* – velocity streamlines in the piece of geometry (**Fig. 3, *b***); *b* – contour plot of the shear stress at the bottom

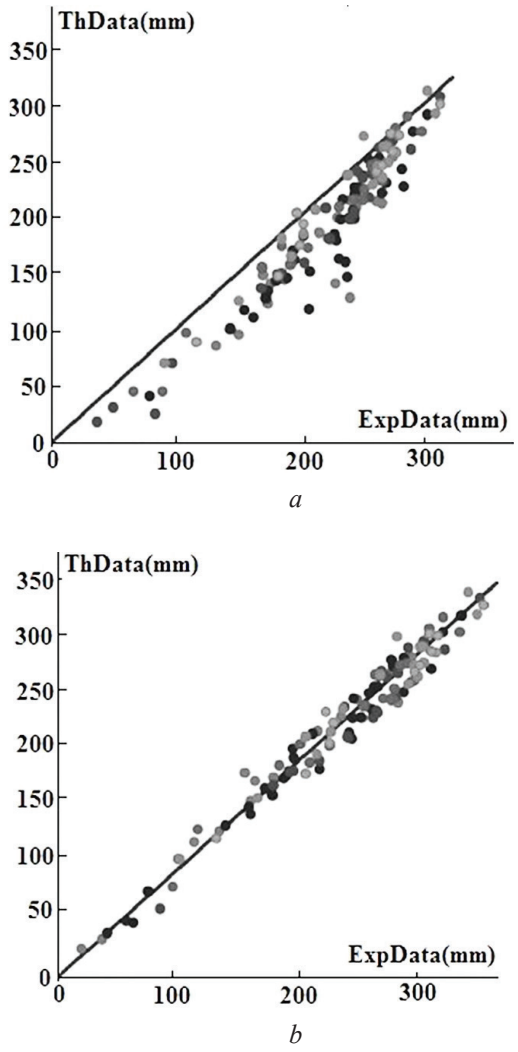

Fig. 7. Statistical distributions ThData vs ExpData over Kharkiv region in 2016−2020: *a* − raw data; *b* − bias-treated data

For each of the probabilistic approximations (10) the likelihood function F_{lkh} can be computed as

$$F_{lkh} = \sum_{j=1}^{n} \ln\left(F_j\left(V, \alpha, \beta, \zeta\right)\right), \tag{11}$$

where n is the number of observations.

The approximations (10) have been computed for the precipitation level h(mm), runoff and surface water flow rates Q(m^3/s), mean air temperature T(°C) and relative humidity (RH) by computations of the best fit parameters α, β, ς with the least square method. The results of approximations for the dependence LHF(Q) are demonstrated in **Fig. 8.**

The best fit approximations for each parameter have been used for numerical computations on (1)–(3) at different possible climate warming scenarios with the mean temperature rise in 0.5; 1; 1.5; 2; 2.5 °C in the year 2040 [1, 2]. Numerical computations on (1)–(3) have been carried out by the finite difference method with accuracy $\varepsilon=10^{-3}$. The results have been validated in known dynamical curves $T(t)$ and $Q(t)$ in 2016–2019 (before the covid-19 pandemic). A good correspondence between the numerical and smoother experimental data has been obtained. The results of

simulations on different scenarios for the total non-dimensional volume $V°$ of water available on the territory of Kharkiv city are presented in **Fig. 9**. The value $V°$ is normalized by the total volume measured in 2019, and the labels in **Fig. 9** show the decrease in the water available relatively to the latest measured value (in July 2019). More recent data for the Ukrainian territory are temporary unavailable.

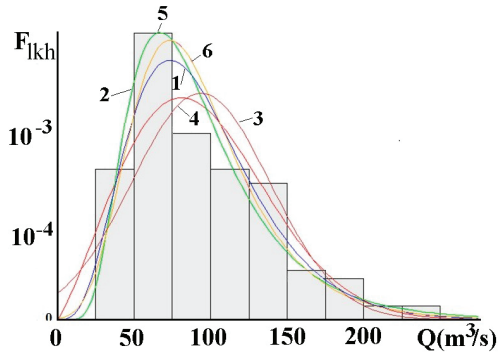

Fig. 8. Dependencies $F_{lkh}(Q)$ and their approximations by the probabilistic functions: 1 – Gamma; 2 – Lognormal; 3 – Normal; 4 – Weibull; 5 – Gumbel; 6 – Gumbel$^+$

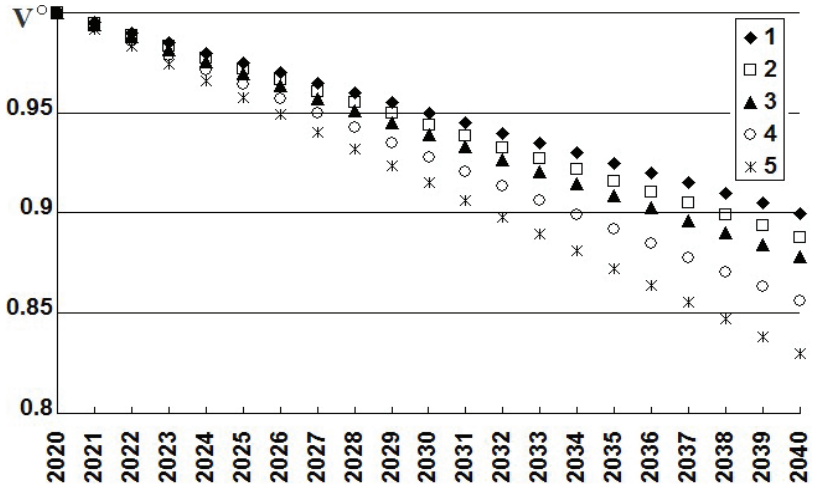

Fig. 9. The non-dimensional dependencies $V°(t)$ prognosed based on the model; the curves 1–5 correspond to the increase in the mean annual air temperature in 2040 by ΔT=0.5; 1; 1.5; 2; 2.5 °C accordingly

According to the computed results, in the worst scenario the water available will be lower in ~20 % (**Fig. 9**). Noticeable variations in the values of the minimum, average, and maximum precipitation rates in different seasons, which could be a result of unpredictable climate changes, do not give the possibility of more accurate numerical prognoses. The latter need more complicated mathematical models with a systems dynamics approach that will be a subject for our further studies.

5. Conclusions

Based on statistical analysis of the meteorological data and measurement results obtained in three rivers (Kharkiv, Lopan, Udy) over the territory of Kharkiv city, it was shown that on the entire territory of Ukraine there is a gradual increase in the average, maximum and minimum annual air temperatures. The differences in the precipitation levels in different months during the year exhibit significant variability: from sudden long-lasting rainfalls to long periods of dryness. The reviewed

regression-probability models are useful for deeper analyzes of the measured data, its approximation by probability functions. The latter can be used as analytical functions in the compartmental hydrological models that allows a reasonable prediction of possible shortage of the drinking water available because of such events like droughts, insufficient capacities of dams and sewage systems in the case of floods, as well as a dangerous gradual increase in the level of pollution in open water sources due to the global weather changes discussed in the work. Direct CFD simulations on real map based geometries give the most detailed results on the river flow velocity and vorticity, shear stress at the river bottom and other values which are important for prognosis of the riverbed evolution (erosion of soils, accumulation and transfer of bottom sediments, plant overgrowth and worsening of water quality). A combination of the regression curves and CFD results with compartmental models allows fast numerical computations of the amount of the drinking and technical water availability for the growing population and industry in large cities at different scenarios of global climate warming.

Conflict of interest

The authors declare that there is no conflict of interest in relation to this paper, as well as the published research results, including the financial aspects of conducting the research, obtaining and using its results, as well as any non-financial personal relationships.

References

[1] Singh, S., Singh, P., Rangabhashiyam, S., Srivastava, K. K. (Eds.) (2021). Global climate change. Elsevier. doi: https://doi.org/10.1016/c2019-0-05200-4

[2] Farooqi, T. J. A., Irfan, M., Portela, R., Zhou, X., Shulin, P., Ali, A. (2022). Global progress in climate change and biodiversity conservation research. Global Ecology and Conservation, 38, e02272. doi: https://doi.org/10.1016/j.gecco.2022.e02272

[3] Verdugo, J., Damm, E., Schaffer, J., Bauch, D., Meyer, H., Kaiser, J. (2022). Impacts of glacier and sea ice melt on methane pathways on the Northeast Greenland shelf. Continental Shelf Research, 243, 104752. doi: https://doi.org/10.1016/j.csr.2022.104752

[4] Huss, M., Schwyn, U., Bauder, A., Farinotti, D. (2021). Quantifying the overall effect of artificial glacier melt reduction in Switzerland, 2005–2019. Cold Regions Science and Technology, 184, 103237. doi: https://doi.org/10.1016/j.coldregions.2021.103237

[5] Du, X., Silwal, G., Faramarzi, M. (2022). Investigating the impacts of glacier melt on stream temperature in a cold-region watershed: Coupling a glacier melt model with a hydrological model. Journal of Hydrology, 605, 127303. doi: https://doi.org/10.1016/j.jhydrol.2021.127303

[6] Pradhananga, D., Pomeroy, J. W. (2022). Diagnosing changes in glacier hydrology from physical principles using a hydrological model with snow redistribution, sublimation, firnification and energy balance ablation algorithms. Journal of Hydrology, 608, 127545. doi: https://doi.org/10.1016/j.jhydrol.2022.127545

[7] Singh, V. P., Frevert, D. K. (2002). Mathematical models of large watershed hydrology. Water Resources Publication, 891.

[8] Sorooshian, S., Hsu, K.-L., Coppola, E., Tomassetti, B., Verdecchia, M., Visconti, G. (Eds.) (2008). Hydrological modelling and the water cycle: Coupling the atmospheric and hydrological models. Springer, 291. doi: https://doi.org/10.1007/978-3-540-77843-1

[9] Kolditz, O., Görke, U.-J., Shao, H., Wang, W. (Eds.) (2012). Thermo-Hydro-Mechanical-Chemical Processes in Porous Media: Benchmarks and Examples. Springer, 399. doi: https://doi.org/10.1007/978-3-642-27177-9

[10] Balabukh, V., Lavrynenko, O., Bilaniuk, V., Mykhnovych, A., Pylypovych, O. (2018). Extreme Weather Events in Ukraine: Occurrence and Changes. Extreme Weather. doi: https://doi.org/10.5772/intechopen.77306

[11] Mamman, M. J., Martins, O. Y., Ibrahim, J., Shaba, M. I. (2017). Evaluation of Best-Fit Probability Distribution Models for the Prediction of Inflows of Kainji Reservoir, Niger State, Nigeria. Air, Soil and Water Research, 10, 117862211769103. doi: https://doi.org/10.1177/1178622117691034

[12] Dincer, I., Colpan, C. O., Kadioglu, F. (Eds.) (2013). Causes, Impacts and Solutions to Global Warming. Springer. doi: https://doi.org/10.1007/978-1-4614-7588-0

[13] Nathan, R., Jordan, P., Scorah, M., Lang, S., Kuczera, G., Schaefer, M., Weinmann, E. (2016). Estimating the exceedance probability of extreme rainfalls up to the probable maximum precipitation. Journal of Hydrology, 543, 706–720. doi: https://doi.org/10.1016/j.jhydrol.2016.10.044

[14] Foufoula-Georgiou, E. (1989). A probabilistic storm transposition approach for estimating exceedance probabilities of extreme precipitation depths. Water Resources Research, 25 (5), 799–815. doi: https://doi.org/10.1029/wr025i005p00799

[15] Schaefer, M. G. (1990). Regional analyses of precipitation annual maxima in Washington State. Water Resources Research, 26 (1), 119–131. doi: https://doi.org/10.1029/wr026i001p00119
[16] Yevjevich, V. (1972). Probability and statistics in hydrology. Water Resources Publications, 302.
[17] Kolditz, O. (2002). Computational Methods in Environmental Fluid Mechanics. Springer, 378. doi: https://doi.org/10.1007/978-3-662-04761-3
[18] Langat, P. K., Kumar, L., Koech, R. (2019). Identification of the Most Suitable Probability Distribution Models for Maximum, Minimum, and Mean Streamflow. Water, 11 (4), 734. doi: https://doi.org/10.3390/w11040734
[19] Sordo-Ward, Á., Granados, I., Martín-Carrasco, F., Garrote, L. (2016). Impact of Hydrological Uncertainty on Water Management Decisions. Water Resources Management, 30 (14), 5535–5551. doi: https://doi.org/10.1007/s11269-016-1505-5
[20] WMO Weather Stations. Available at: https://www.arcgis.com/home/item.html?id=c3cbaceff97544a1a4df93674818b012
[21] World Climate. Data Basin. Available at: https://databasin.org/
[22] World Weather database. Available at: https://worldweather.wmo.int/en/home.html

Received date 03.06.2022
Accepted date 10.07.2022
Published date 31.07.2022

How to cite: *Rychak, N., Kizilova, N. (2022). Mathematical modeling of drinking water availability in Kharkiv region (Ukraine) at different dynamics of global climate warming. EUREKA: Life Sciences, 4, 21–34. doi: https://doi.org/10.21303/2504-5695.2022.002610*